AGU PUBLICATIONS

Geophysical Research Letters

RESEARCH LETTER
10.1002/2015GL064208

Key Points:
- Fault Zone Guided Waves observed within the late interseismic Alpine Fault
- Transpressional Alpine Fault zone comparable at depth to San Andreas Fault

Supporting Information:
- Text S1, Figures S1–S3, and Table S1

Correspondence to:
J. D. Eccles,
j.eccles@auckland.ac.nz

Citation:
Eccles, J. D., A. K. Gulley, P. E. Malin, C. M. Boese, J. Townend, and R. Sutherland (2015), Fault Zone Guided Wave generation on the locked, late interseismic Alpine Fault, New Zealand, *Geophys. Res. Lett.*, *42*, 5736–5743, doi:10.1002/2015GL064208.

Received 12 APR 2015
Accepted 23 JUN 2015
Accepted article online 25 JUN 2015
Published online 16 JUL 2015

©2015. American Geophysical Union. All Rights Reserved.

Fault Zone Guided Wave generation on the locked, late interseismic Alpine Fault, New Zealand

J. D. Eccles[1], A. K. Gulley[2], P. E. Malin[3], C. M. Boese[4], J. Townend[5], and R. Sutherland[5,6]

[1]School of Environment, University of Auckland, Auckland, New Zealand, [2]Department of Mathematics, University of Auckland, Auckland, New Zealand, [3]Department of Physics, University of Auckland, Auckland, New Zealand, [4]International Earth Sciences IESE Ltd., Auckland, New Zealand, [5]School of Geography, Environment and Earth Sciences, Victoria University of Wellington, Wellington, New Zealand, [6]GNS Science, Lower Hutt, New Zealand

Abstract Fault Zone Guided Waves (FZGWs) have been observed for the first time within New Zealand's transpressional continental plate boundary, the Alpine Fault, which is late in its typical seismic cycle. Ongoing study of these phases provides the opportunity to monitor interseismic conditions in the fault zone. Distinctive dispersive seismic codas (~7–35 Hz) have been recorded on shallow borehole seismometers installed within 20 m of the principal slip zone. Near the central Alpine Fault, known for low background seismicity, FZGW-generating microseismic events are located beyond the catchment-scale partitioning of the fault indicating lateral connectivity of the low-velocity zone immediately below the near-surface segmentation. Initial modeling of the low-velocity zone indicates a waveguide width of 60–200 m with a 10–40% reduction in *S* wave velocity, similar to that inferred for the fault core of other mature plate boundary faults such as the San Andreas and North Anatolian Faults.

1. Introduction

The ~850 km long Alpine Fault, New Zealand, is a transpressional continental plate boundary structure accommodating most of the relative motion between the Australian and Pacific plates [*Norris and Cooper*, 2001]. It has accumulated total dextral offset of 440–470 km [*Sutherland*, 1999] with a current rate of 27 ± 5 mm/yr strike slip [*Norris and Cooper*, 2001; *Sutherland*, 1999]. Uplift, currently 10 mm/yr, has exhumed hanging wall mylonites from ~20 km depth [*Cooper and Norris*, 1994]. The fault dips 45–60°SE [*Sibson et al*., 1981], and while appearing linear from the air, closer mapping reveals thrust and strike-slip partitioning on a catchment (<5 km) scale thought to be associated with large along-strike variations in topography and hence stress [*Norris and Cooper*, 1995; *Barth et al*., 2012].

The Alpine Fault has not ruptured historically; however, paleoseismicity on the southern portion of the Alpine Fault reveals a pattern of 24 large events with an average recurrence time of 329 ± 68 years [*Berryman et al*., 2012]. The last large (> *M*8) earthquake on the central Alpine Fault occurred in 1717 A.D. [*Wells et al*., 1999], and hence, the Alpine Fault is considered to be late in its seismic cycle.

The central Alpine Fault is a region of anomalously low background microseismicity [*Boese et al*., 2012; *Bourguignon et al*., 2015]. The spatial variations in current seismicity observed in the central Southern Alps and localized seismic tremor and low-frequency earthquakes are indicative of variable fluid and stress conditions near the fault [*Boese et al*., 2012; *Wech et al*., 2012; *Boese et al*., 2014; *Chamberlain et al*., 2014].

Mature faults, such as the San Andreas Fault, North Anatolian Fault, and Dead Sea Transform, exhibit Fault Zone Guided Wave (FZGW) phases within the seismic coda [*Ben-Zion et al*., 2003; *Haberland et al*., 2003; *Li and Malin*, 2008; *Ellsworth and Malin*, 2011]. These phases are also observed in recently ruptured low slip rate fault systems such as Canterbury [*Li et al*., 2014] and have been attributed to a low-velocity zone (LVZ) waveguide caused by damage within the fault zone [*Wu et al*., 2008; *Lewis and Ben-Zion*, 2010; *Ellsworth and Malin*, 2011]. Fault Zone Head Waves may also be associated with a biomaterial interface across a fault [*Bulut et al*., 2012]. The trapped waves are characterized by dispersive coda, variously of trapped *P-SV* types (denoted by F_R) and trapped *SH* (F_L) phases that follow the *S* wave arrival [*Malin et al*., 1996]. Less commonly observed are leaky-*P-SV* phases (F_Φ), appearing between the *P* and *S* wave arrivals [*Ellsworth and Malin*, 2011].

Dispersion of FZGWs is a consequence of the angle of internal reflection for each frequency; the trapped high frequencies reflect at steeper angles, have longer raypaths, and hence travel at slower phase velocities

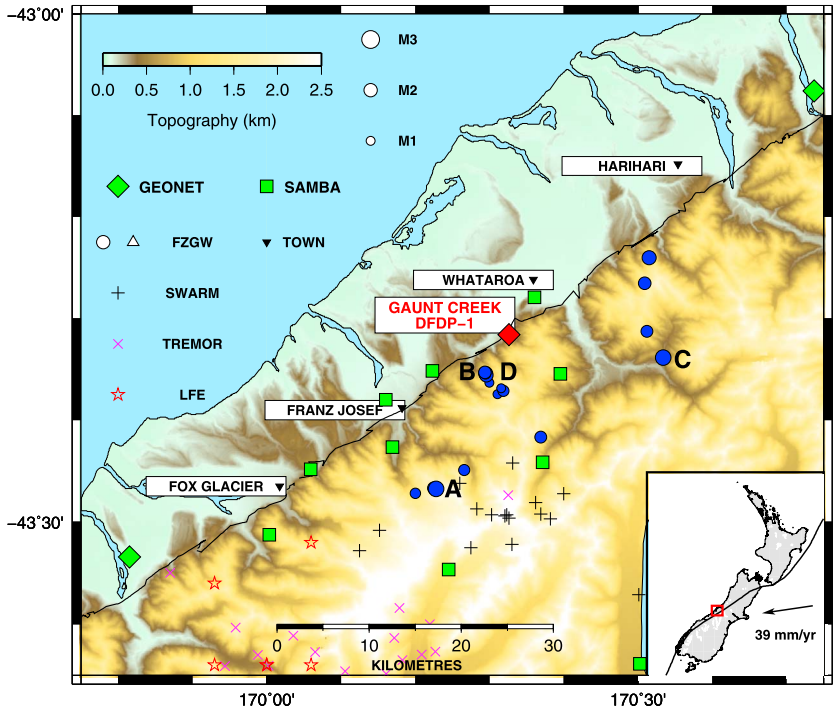

Figure 1. Map of South Westland. The Alpine Fault is shown by the black line with the location of DFDP-1 drilling at Gaunt Creek indicated by the red diamond. Green symbols represent seismometers in operation for the time period discussed (diamonds: GeoNet stations [*Petersen et al.*, 2011]; filled squares: SAMBA [*Boese et al.*, 2012]). Microseismic events identified to have produced FZGW are plotted as dots with the size indicative of magnitude as indicated in the legend; triangles represent located FZGW-generating events without calculated magnitudes. Location uncertainty is event dependent as discussed in *Boese et al.* [2012] and shown in Table S1. Black plus symbols represent microearthquake swarms [*Boese et al.*, 2014], pink cross symbols represent tremor located at 10–65 km depth [*Wech et al.*, 2012], and open red stars represent low-frequency earthquakes located at 18–28 km depth [*Chamberlain et al.*, 2014]. Labels A–D refer to events illustrated in later figures. Inset: location of main map within New Zealand with the plate boundary and relative motion shown.

[*Ben-Zion*, 1998]. While the exact range of possible source locations relative to the waveguide remains subject to debate [*Li and Malin*, 2008; *Wu et al.*, 2008], the observed FZGWs are strongest when source and receiver are at, close to, or beneath the waveguide. Patterns of FZGW generation and observation can be used to interpret the connectivity of the fault with depth [*Jahnke et al.*, 2002]. Modeling of these phases can be used to infer the velocity and geometry of the damage zone [*Ben-Zion*, 1998; *Li and Malin*, 2008], yielding to insights about rupture processes [*Kuwahara and Ito*, 2002].

The Deep Fault Drilling Project (DFDP) is an initiative to explore the in situ properties of the late interseismic, crustal-scale Alpine Fault where rapid uplift rates facilitate drilling of the seismogenic zone [*Townend et al.*, 2009; *Sutherland et al.*, 2012]. The first phase of shallow drilling, DFDP-1, occurred at Gaunt Creek (Figure 1) with two wells intersecting the principal slip zone (PSZ) [*Sutherland et al.*, 2012; *Townend et al.*, 2013]. The boreholes were cored and geophysical well logs, including full-waveform sonic and density logs, collected [*Sutherland et al.*, 2012; *Townend et al.*, 2013; *Toy et al.*, 2015].

The DFDP-1 borehole observatory [*Sutherland et al.*, 2012] included gimbaled three-component 2 Hz borehole sondes. These were installed 10 m above and 10 m below the shallowest principal slip zone identified; at 81 m in DFDP-1A and 139 m DFDP-1B, ~100 m apart. These borehole seismometers are well suited to recording FZGW phases as they are located beneath the highly attenuating low-velocity alluvial gravels. Such overburden units are known to disrupt the waveguide and inhibit or complicate the recording of FZGWs on surface stations [*Li and Vidale*, 1996].

In this paper we analyze data, sampled at 200 Hz, collected over 125 days between February and July 2011 to identify and interpret potential FZGWs. In July 2011, a lightning strike disabled the seismometers and while the shallower DFDP-1A instrument was replaced with an identical unit, the cemented-in DFDP-1B

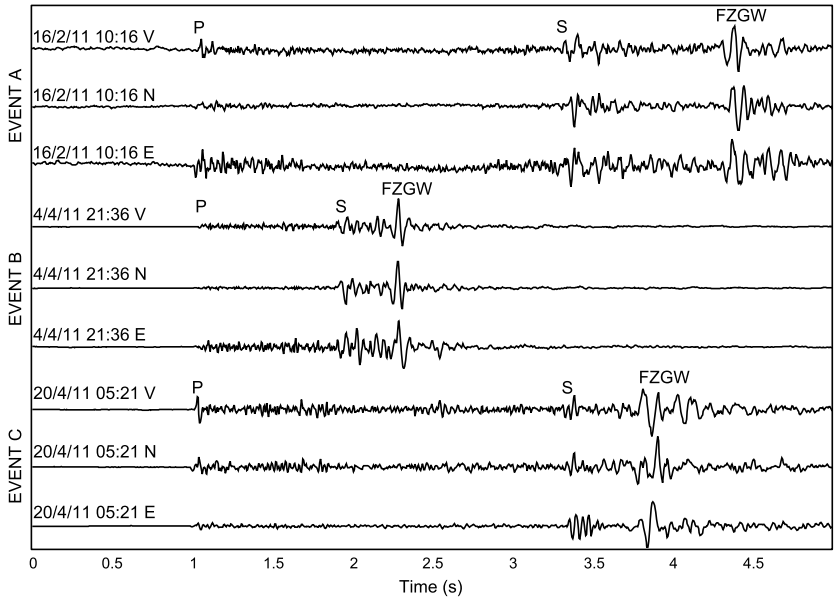

Figure 2. Seismograms recorded in the DFDP-1A borehole for Events A–C (Figure 1), illustrating FZGW phases. Events A–C occurred on 16 February, 4 April, and 20 April 2011 respectively. Seismograms are aligned on the *P* wave arrival. Seismogram amplitudes have been normalized with the vertical axis showing the frequencies of the spectrogram. The horizontal components have been rotated to the north and east using blasts from the nearby Whataroa quarry.

seismometer could not be replaced. The New Zealand national network, GeoNet [*Petersen et al*., 2011], provides ongoing telemetry of the DFDP-1A borehole seismometer.

2. Observations

The DFDP-1 seismometers produced high-quality waveforms from both local and regional seismic events. Installation of instruments took place 11 days before the disastrous 22 February 2011 M_w6.2 Christchurch earthquake occurred ~200 km away [*Kaiser et al*., 2012]. During the 125 days of operation, 1179 earthquakes, dominated by Christchurch aftershocks, were observed on the Gaunt Creek seismometers with *S-P* times exceeding 10 s. More locally, 604 events were observed with *S-P* times of 1–10 s and 140 with *S-P* times of less than 1 s.

The shallower DFDP-1A seismometer, sanded in 10 m above the PSZ, typically had a higher signal-to-noise ratio than the one cemented in beneath the PSZ in DFDP-1B. We hypothesize that this unexpected effect reflects a bias of event locations in the hanging wall [*Boese et al*., 2012] and signal attenuation/scattering across the fault zone. Drilling revealed progressive fracturing and alteration extending $>$ 100 m into the hanging wall, although both sensors were located within clay-cemented cataclasites [*Sutherland et al*., 2012; *Townend et al*., 2013; *Toy et al*., 2015]. Another explanation may be differential interaction with the free-surface ghost [*Schuster et al*., 2004].

Nearby earthquakes were located using stations from GeoNet and the short-period Southern Alps Microearthquake Borehole Array (SAMBA) [*Boese et al*., 2012] using the approach of *Boese et al*. [2012]. These locations are shown in Figure 1 and detailed in Table S1 in the supporting information. Seventy-six FZGW events with *S-P* times of up to 4.5 s were located. There were also many potential low-amplitude, short *S-P* time FZGW-generating events observed at DFDP-1 that were unable to be located.

FZGW examples are shown in Figure 2. These high signal-to-noise ratio events, located at points A–C in Figure 1 near the interpreted fault plane, are characterized by distinct *P* and *S* wave arrivals followed by dispersive arrivals that typically have amplitudes in excess of those of the body waves. Surface waves also show dispersion, but for earthquakes of these magnitudes and source-receiver geometries discernable surface wave amplitudes would not be expected [*Aki and Richards*, 2002]. Moreover, surface waves for these events are not observed on nearby surface and borehole sensors such as those of the SAMBA array. Rotation

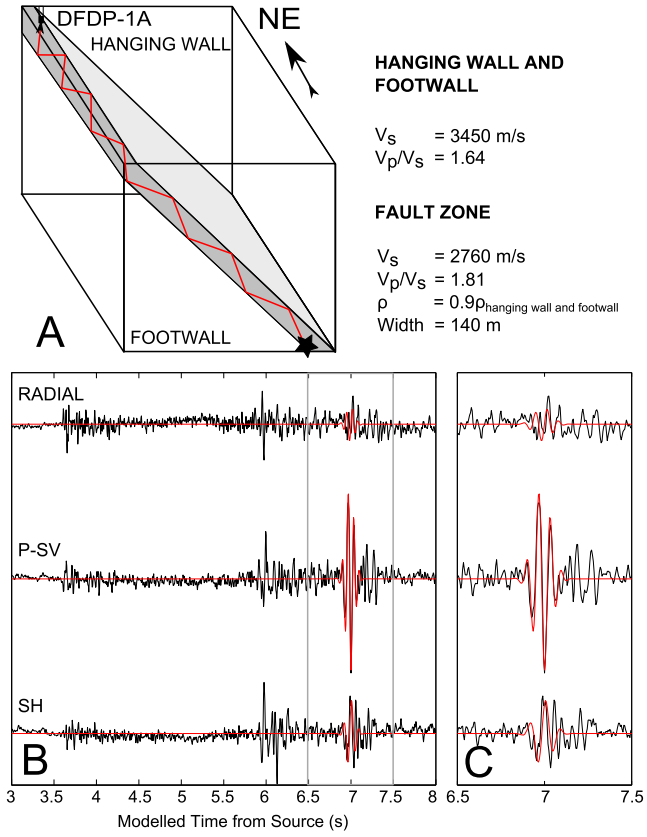

Figure 3. Full elastic forward modeling of FZGWs for the event on 16 February 2011 (location A, Figure 1). (a) Schematic of the three-layer model used, including the assumed and modeled physical properties. (b) The observed coda of the FZGWs (black) is matched by the modeled waveforms (red). Note that data have been rotated into radial and transverse (*P-SV* and *SH*) components. (c) Zoom of boxed portion in Figure 3b showing the FZGW coda.

of the FZGW arrivals into radial and transverse components reveals that many of the dispersed signals have partitioning that can be ascribed to F_R modes [*Malin et al.*, 1996]. The deeper Event C is anomalous of the events observed with more F_L waves and a delay time less than that observed for shallower events at a similar hypocentral distance.

Microearthquake swarms have been previously reported within the region [*Boese et al.*, 2014]. Within the February–July 2011 catalogue of FZGW events, two swarms were observed, including an early April swarm of 16 events in 9 days (Figure S1). The normalized maximum cross-correlation coefficients, occurring within the picking uncertainty of aligned *P* wave arrivals, have a mean value of 0.78 and standard deviation of 0.10. The amplitude of the largest phase (FZGW) within the coda of different events within this swarm varies by a factor of 40. Events with sufficient signal-to-noise ratio on the array to enable extensive picking were located 7–13 km deep beneath Purcell Creek, Location D in Figure 1, with a local magnitude of 1.7–2.5.

3. Modeling

The Alpine Fault FZGW events contain energy at frequencies of 1–60 Hz with clear dispersion 7–35 Hz. There is significant loss of higher frequencies through attenuation with increasing source to receiver distance [e.g., *Ellsworth and Malin*, 2011]. The frequencies observed within FZGWs are controlled by the waveguide properties [*Wu et al.*, 2008] and location of the source and receiver relative to the waveguide [*Jahnke et al.*, 2002]. The lower frequency limit may be influenced by the response of the short-period (2 Hz) borehole seismometer; however, little energy is observed at frequencies lower than 5–8 Hz, meaning this appears to have little impact on the coda. This is in contrast to some surface recordings from the San Andreas Fault in which low-pass filtering has been performed prior to waveform modeling ($<$4 Hz [*Li et al.*, 1997]; $<$ 5 and 8 Hz [*Li and Malin*, 2008]). In the case of the Calico Fault, California, modeling of FZGWs at frequencies lower than 2 Hz was performed to match the 1.5 km wide damage zone modeled using geodetic data [*Cochran et al.*, 2009].

We performed elastic modeling of selected FZGWs using the Green's functions for a point source [*Aki and Richards*, 2002]. The fault zone was modeled as three layers, a low-velocity fault "damage zone" sandwiched between uniform wall rocks as shown in Figure 3a. The latter represents the footwall and hanging wall whose velocities were constrained by (1) laboratory measurements [*Christensen and Okaya*, 2007], (2) active source studies of the region [*van Avendonk et al.*, 2004], and (3) regional earthquake seismology [*Eberhart-Phillips and Bannister*, 2002]. Little is known about properties of the fault zone itself at depth, so the starting model was informed by the DFDP-1 well logs [*Townend et al.*, 2013] and V_p/V_s ratios observed in similar faults elsewhere [*Li et al.*, 2004; *Hung et al.*, 2009].

Figures 3b and 3c show the modeled fit of the Event A shown in Figure 2 using a model with a 140 m wide LVZ and an *S* wave velocity reduction of ~20%. The normalized model-to-data cross correlation is 0.7. Events

B and C are fitted similarly (Figures S2 and S3) with 100 m and 125 m widths and 25% and 15% velocity reductions, respectively. A predominantly strike slip source mechanism, consistent with what could be expected on the Alpine Fault, was found to account for observed F_L and F_R waves. A LVZ of such dimensions is consistent with those seen in the mature, continental plate boundaries of the San Andreas and North Anatolian Faults [*Li and Malin*, 2008; *Ben-Zion et al*., 2003].

The dispersion of FZGW-generating events with hypocentral distance uncertainties less than 2.5 km were also modeled using windowed Fourier transforms following the approach of *Wu and Hole* [2011]. These models, tabulated in Table S1, indicate that the low-velocity zone of the Alpine Fault has a width of 60–200 m and *S* wave velocity contrast compared to the hanging wall of 10–40%. As width and velocity contrast trade off, a narrow fault width corresponds to greater velocity contrast. The fitting criterion is to be within 50% of the amplitude of the peak frequency of the windowed Fourier transform. This approximately corresponds to ±3 Hz.

4. Discussion

The relationship of a "low-velocity" damage zone inferred from FZGW observations has not been definitively or generically tied to geology at depth. The ~200 m wide San Andreas Fault zone intersected in San Andreas Fault Observatory at Depth drilling and, consistent with that modeled with FZGW data [*Ellsworth and Malin*, 2011], was defined on the basis of *P* wave, *S* wave, and resistivity well logs with the margins of this zone also corresponding to lithological boundaries and defined faults which could be expected to focus deformation [*Zoback et al*., 2011]. At the lower offset Calico Fault, California, which has not ruptured historically, the geodetically and FZGW-modeled damage zone is 1.5 km wide, an order of magnitude wider than that commonly observed on more recently ruptured faults [*Cochran et al*., 2009]. The broader damage zone observed could be a consequence of the maturity or geometry of the fault (e.g., branching) or simply a wide, lower intensity, damage zone that would be seen around the more intensive zone of deformation of a more recently ruptured fault [*Cochran et al*., 2009].

The extent and character of even the shallow damage zone of the Alpine Fault is unknown as surface outcrops and the section drilled and logged in DFDP-1 are limited [*Townend et al*., 2013; *Toy et al*., 2015]. DFDP-1 drilling beneath the gravel overburden was entirely within the fractured damage zone; well logs and laboratory measurements captured only small-scale velocity and density anomalies associated with the principal slip zone such as the low-velocity and low-density fault gouge and fractures and higher-velocity and higher-density clay-cemented cataclasites [*Townend et al*., 2013]. At Gaunt Creek competent rock at the surface is only found at significant distance from the principal slip zone [*Cooper and Norris*, 1994]. The highly fractured hanging wall mylonites seen near the fault core would be hypothesized to have lower velocity and density than their unfractured equivalent further from the fault as seen at the San Andreas Fault [*Zoback et al*., 2011]. The surface deformation/fracturing could be expected to be wider than the low-velocity waveguide at depth due to confining pressure, weathering, brittle deformation duration with uplift [e.g., *Lund Snee et al*., 2014], and the potential development of flower structures [*Finzi et al*., 2009]. Little is known of the brittle deformation of the Alpine Fault footwall; only ~12 m was logged during DFDP-1 adjacent to the principal slip zone [*Townend et al*., 2013]. Although rare surface outcrops do exist [e.g., *Lund Snee et al*., 2014], spatial separation of these from the Alpine Fault hinder interpretation of the character of the LVZ in the footwall.

The Alpine Fault zone at depth is thought to occur between hard rocks; predominantly quartzo-feldspathic protolith derived mylonitic sequences in the hanging wall [*Cooper and Norris*, 1994] and the largely plutonic and gneissic rocks of the footwall [*Cox and Barrell*, 2007]. The Alpine Fault shows evidence for multiple or migrating shallow PSZs [*Sutherland et al*., 2012] and for the entrainment of footwall material into the fault zone at different depths [e.g., *Toy et al*., 2015]. The nature of the seismically defined LVZ at depth, whether a sharply bounded zone between splays of the fault or a fractured, and potentially altered, zone defined by a critical density of connected fractures is thus unclear [*Leary*, 1991; *Finzi et al*., 2009]. Another possibility to be explored for the Alpine Fault setting is the potential role of the seismic anisotropy associated with the metamorphic fabric [*Christensen and Okaya*, 2007]. This property may extend beyond the brittle deformation itself, although at great depth shear wave splitting shows anisotropy is broadly distributed [*Karalliyadda and Savage*, 2013].

Healing of the damage zone, restoring its elastic properties, would be expected as fractures opened coseismically close. The last known rupture of the central Alpine Fault occurred in 1717 A.D. [*Wells et al*., 1999], yet a LVZ

capable of propagating FZGWs has been retained until today, late in the interseismic cycle. The Landers Fault showed ~2.5% recovery of seismic *P* and *S* wave velocities within the damage zone in the decade following the 1992 Landers earthquake [*Vidale and Li*, 2003]. The San Andreas Fault at Parkfield recovered ~1% of an estimated coseismic 2.5% velocity drop in 3 months [*Li et al*., 2006]. Such findings are in contrast to FZGW and geodetically modeled damage zones in California with velocities 10–50% lower than the surrounding country rock [*Cochran et al*., 2009; *Ellsworth and Malin*, 2011; *Li and Malin*, 2008]. Hence, the damage associated with, and able to be healed with, individual seismic cycles is minor compared to permanent damage occurring close to the fault core in the mature faults studied. The efficiency of healing is thought to relate to the fault segmentation with unsegmented faults demonstrating well developed, enduring damage zones and fault rocks [*Finzi et al*., 2011].

The FZGW-inducing events observed are largely located between Harihari in the north and Fox Glacier in the south, i.e., within 20 km of Gaunt Creek, with depths ranging between 1 and 12 km. Segmentation of the Alpine Fault is observed at the catchment-scale along strike (1–5 km) and has been hypothesized to extend to 1–2 km depth [*Norris and Cooper*, 1995; *Barth et al*., 2012]. Initial results indicate that FZGWs are observed from earthquakes as large as M_L3 located across the segment boundary in the Whataroa Valley 8 km northeast of Gaunt Creek. This may indicate that the seismic waveguide is continuous below the near-surface segmentation. However, hypocentral distance versus *S* wave to FZGW delay time analysis shows that events deeper than ~8 km (e.g., Event C) have shorter delays than shallower events, possibly indicating that they occur below a LVZ of finite depth extent [*Lewis et al*., 2005; *Wu et al*., 2008]. The near lack of small ($< M_L1$), shallow events beyond the single Alpine Fault segment in the local catchment may indicate that the deformation zone in the shallow Alpine Fault is discontinuous in the near surface to as much as 4 km depth but could also be an artifact of attenuation.

Earthquake swarms, tectonic tremor, and low-frequency earthquakes have recently been observed in the Southern Alps/Alpine Fault region [*Wech et al*., 2012; *Boese et al*., 2014; *Chamberlain et al*., 2014] and are thought to be associated with (1) the movement of fluids [*Vidale and Shearer*, 2006], (2) aseismic creep [*Roland and McGuire*, 2009], or (3) slow slip [*Wech et al*., 2012]. These events are concentrated southwest of and at greater depths than the DFDP-1 FZGW events that cluster 5 km SW of Gaunt Creek (Figure 1). While not showing the intensity of microseismicity observed farther south [*Boese et al*., 2014], this FZGW-generating patch can be more confidently attributed to activity on/ very near or beneath [*Li and Vidale*, 1996; *Ben-Zion et al*., 2003; *Li and Malin*, 2008; *Wu et al*., 2008] the damage zone of the Alpine Fault itself. On the North Anatolian Fault, *Ben-Zion et al*. [2003] observed FZGWs generated from a large number of off-fault events at depth. This is modeled to be the effect of a shallow waveguide and is also a possibility for the dipping Alpine Fault, although it has low rates of footwall seismicity [*Boese et al*., 2012].

The DFDP-1A borehole seismometer in the Alpine Fault zone is ideally positioned to record seismicity until (and ideally beyond) rupture. This provides an opportunity to monitor seismicity through time and investigate foreshock and aftershock activity. Seismicity rates in Japan have been observed to accelerate in an inverse Omari's law [*Peng et al*., 2007] prior to earthquakes, and the additional monitoring of FZGW on a structure due to rupture will allow rates and waveform characteristics indicative of changing fault zone properties to be investigated in more detail on an ongoing basis [*Peng and Ben-Zion*, 2006; *Calderoni et al*., 2015].

5. Conclusions

The first observations of Fault Zone Guided Waves on the Alpine Fault of New Zealand have been made. Three-layer modeling yields a low-velocity waveguide with a thickness of approximately 60–200 m and ~10–40% reduction in *S* wave velocity within the brittle crust that is consistent with those seen at other mature, continental plate boundary faults. Outcrop and borehole studies on the Alpine Fault are consistent with this waveguide corresponding to the fractured damage zone of the fault.

The propagation of FZGW indicates that the fault is continuous at depth between shallow (<8 km) hypocenter locations and the DFDP-1 boreholes in a region with evidence for catchment-scale (1–5 km) segmentation at the surface. However, events > 8 km show shorter FZGW delays indicative of a waveguide with limited depth. The location of FZGW-generating microseismicity, including swarms, is consistent with hypothesized location of the southeastward dipping fault plane and indicative of seismicity on, near, or below the fault zone. The presence of FZGW provides the opportunity to perform more detailed modeling of the fault zone properties,

and longer-period catalogues will enable enhanced spatiotemporal analysis of seismicity on the fault. As the Alpine Fault is late in its seismic cycle, ongoing monitoring of near-fault seismicity could provide insight into changing fault zone properties and behavior before the next earthquake and, should the installation survive, during and following rupture.

Acknowledgments

Raw waveform data are available on request to the corresponding author. Data plotted in Figure 1 are tabulated in supporting information Table S1 and additional modeling shown in Figures S2 and S3. Drilling operations were made possible by Horizon Drilling, Alex Pyne, New Zealand Department of Conservation, Whataroa Community, GNS Science, Deutsche Forschungsgemeinschaft, National Environment Research Council grant NE/H012486/1, and the following universities: Victoria University of Wellington, Otago, Auckland, Canterbury, Bremen, and Liverpool. Marsden grant UOA1012 supported this research. Discussions with the wider DFDP-1 and DFDP-2 communities have helped to shape this research. Constructive reviews were provided by M. Bohnhoff and an anonymous reviewer.

The Editor thanks Marco Bohnhoff and an anonymous reviewer for their assistance in evaluating this paper.

References

Aki, K., and P. G. Richards (2002), *Quantitative Seismology*, 700 pp., Univ. Science Books, Sausalito, Calif.

Barth, N. C., V. G. Toy, R. M. Langridge, and R. J. Norris (2012), Scale dependence of oblique plate-boundary partitioning: New insights from LiDAR, central Alpine fault, New Zealand, *Lithosphere*, *4*(5), 435–448, doi:10.1130/L201.1.

Ben-Zion, Y. (1998), Properties of seismic fault zone waves and their utility for imaging low-velocity structures, *J. Geophys. Res.*, *103*(B6), 12,567–12,585, doi:10.1029/98JB00768.

Ben-Zion, Y., Z. Peng, D. A. Okaya, L. Seeber, J. G. Armbruster, N. Ozer, A. J. Michael, S. Baris, and M. Aktar (2003), A shallow fault-zone structure illuminated by trapped waves in the Karadere-Duzce branch of the North Anatolian Fault, western Turkey, *Geophys. J. Int.*, *152*(3), 699–717.

Berryman, K. R., U. A. Cochran, K. J. Clark, G. P. Biasi, R. M. Langridge, and P. Villamor (2012), Major earthquakes occur regularly on an isolated plate boundary fault, *Science*, *336*(6089), 1690–1693, doi:10.1126/science.1218959.

Boese, C. M., J. Townend, E. Smith, and T. Stern (2012), Microseismicity and stress in the vicinity of the Alpine Fault, central Southern Alps, New Zealand, *J. Geophys. Res.*, *117*, B02302, doi:10.1029/2011JB008460.

Boese, C. M., K. M. Jacobs, E. G. C. Smith, T. A. Stern, and J. Townend (2014), Background and delayed-triggered swarms in the central Southern Alps, South Island, New Zealand, *Geochem. Geophys. Geosyst.*, *15*, 945–964, doi:10.1002/2013GC005171.

Bourguignon, S., S. Bannister, C. M. Henderson, J. Townend, and H. Zhang (2015), Structural heterogeneity of the mid-crust adjacent to the central Alpine Fault, New Zealand: Inferences from seismic tomography and seismicity between Harihari and Ross, *Geochem. Geophys. Geosyst.*, *16*, 1017–1043, doi:10.1002/2014GC005702.

Bulut, F., Y. Ben-Zion, and M. Bohnhoff (2012), Evidence for a bimaterial interface along the Mudurnu segment of the North Anatolian fault zone from polarization analysis of P waves, *Earth Planet. Sci. Lett.*, *327–328*, 17–22, doi:10.1016/j.epsl.2012.02.001.

Calderoni, G., A. Rovelli, and R. Di Giovambattista (2015), Transient anomaly in fault zone-trapped waves during the preparatory phase of the 6 April 2009, M_w 6.3 L'Aquila earthquake, *Geophys. Res. Lett.*, *42*, 1750–1757, doi:10.1002/2015GL063176.

Chamberlain, C. J., D. R. Shelly, J. Townend, and T. A. Stern (2014), Low-frequency earthquakes reveal punctuated slow slip on the deep extent of the Alpine Fault, New Zealand, *Geochem. Geophys. Geosyst.*, *15*, 2984–2999, doi:10.1002/2014GC005436.

Christensen, N. I., and D. A. Okaya (2007), Compressional and shear wave velocities in *South Island, New Zealand Rocks and Their Application to the Interpretation of Seismological Models of the New Zealand Crust*, *Geophys. Monogr. Ser.*, vol. 175, edited by D. A. Okaya, T. Stern, and F. J. Davey, pp. 123–155, AGU, Washington, D. C.

Cochran, E. S., Y. Li, P. M. Shearer, S. Barbot, Y. Fialko, and J. E. Vidale (2009), Seismic and geodetic evidence for extensive, long-lived fault damage zones, *Geology*, *37*(4), 315–318, doi:10.1130/G25306A.1.

Cooper, A. F., and R. J. Norris (1994), Anatomy, structural evolution, and slip rate of a plate-boundary thrust: The Alpine Fault at Gaunt Creek, Westland, New Zealand, *Geol. Soc. Am. Bull.*, *106*(5), 627–633.

Cox, S. C., and D. J. A. Barrell (2007), Geology of the Aoraki area, 1:250,000, 71 p. + 1 folded map.

Eberhart-Phillips, D., and S. Bannister (2002), Three-dimensional crustal structure in the Southern Alps region of New Zealand from inversion of local earthquake and active source data, *J. Geophys. Res.*, *107*(B10), 2262, doi:10.1029/2001JB000567.

Ellsworth, W. L., and P. E. Malin (2011), Deep rock damage in the San Andreas Fault revealed by P- and S-type fault-zone-guided waves, *Geol. Soc. London Spec. Publ.*, *359*, 39–53, doi:10.1144/SP359.3.

Finzi, Y., E. H. Hearn, Y. Ben-Zion, and V. Lyakhovsky (2009), Structural properties and deformation patterns of evolving strike-slip faults: Numerical simulations incorporating damage rheology, *Pure Appl. Geophys.*, *166*(10–11), 1537–1573, doi:10.1007/s00024-009-0522-1.

Finzi, Y., E. H. Hearn, V. Lyakhovsky, and L. Gross (2011), Fault-zone healing effectiveness and the structural evolution of strike-slip fault systems, *Geophys. J. Int.*, *186*(3), 963–970, doi:10.1111/j.1365-246X.2011.05099.x.

Haberland, C., A. Agnon, R. El-Kelani, N. Maercklin, I. Qabbani, G. Ruempker, T. Ryberg, F. Scherbaum, and M. Weber (2003), Modeling of seismic guided waves at the Dead Sea Transform, *J. Geophys. Res.*, *108*(B7), 2342, doi:10.1029/2002JB002309.

Hung, J., K. Ma, C. Wang, H. Ito, W. Lin, and E. Yeh (2009), Subsurface structure, physical properties, fault-zone characteristics and stress state in scientific drill holes of Taiwan Chelungpu Fault Drilling Project, *Tectonophysics*, *466*(3–4), 307–321, doi:10.1016/j.tecto.2007.11.014.

Jahnke, G., H. Igel, and Y. Ben-Zion (2002), Three-dimensional calculations of fault-zone-guided waves in various irregular structures, *Geophys. J. Int.*, *151*(2), 416–426, doi:10.1046/j.1365-246X.2002.01784.x.

Kaiser, A., et al. (2012), The M_w 6.2 Christchurch earthquake of February 2011: Preliminary report, *N. Z. J. Geol. Geophys.*, *55*(1), 67–90, doi:10.1080/00288306.2011.641182.

Karalliyadda, S. C., and M. K. Savage (2013), Seismic anisotropy and lithospheric deformation of the plate-boundary zone in South Island, New Zealand: Inferences from local S-wave splitting, *Geophys. J. Int.*, *193*(2), 507–530, doi:10.1093/gji/ggt022.

Kuwahara, Y., and H. Ito (2002), Fault low velocity zones deduced by trapped waves and their relation to earthquake rupture processes, *Earth Planets Space*, *54*(11), 1045–1048.

Leary, P. (1991), Deep borehole log evidence for fractal distribution of fractures in crystalline rock, *Geophys. J. Int.*, *107*(3), 615–627.

Lewis, M. A., and Y. Ben-Zion (2010), Diversity of fault zone damage and trapping structures in the Parkfield section of the San Andreas Fault from comprehensive analysis of near fault seismograms, *Geophys. J. Int.*, *183*(3), 1579–1595, doi:10.1111/j.1365-246X.2010.04816.x.

Lewis, M., Z. Peng, Y. Ben-Zion, and F. Vernon (2005), Shallow seismic trapping structure in the San Jacinto fault zone near Anza, California, *Geophys. J. Int.*, *162*(3), 867–881, doi:10.1111/j.1365-246X.2005.02684.x.

Li, Y., and P. E. Malin (2008), San Andreas Fault damage at SAFOD viewed with fault-guided waves, *Geophys. Res. Lett.*, *35*, L08304, doi:10.1029/2007GL032924.

Li, Y., and J. E. Vidale (1996), Low-velocity fault-zone guided waves: Numerical investigations of trapping efficiency, *Bull. Seismol. Soc. Am.*, *86*(2), 371–378.

Li, Y., W. L. Ellsworth, C. H. Thurber, P. E. Malin, and K. Aki (1997), Fault-zone guided waves from explosions in the San Andreas Fault at Parkfield and Cienega Valley, California, *Bull. Seismol. Soc. Am.*, *87*(1), 210–221.

Li, Y., P. Chen, E. S. Cochran, J. E. Vidale, and T. Burdette (2006), Seismic evidence for rock damage and healing on the San Andreas Fault associated with the 2004 *M* 6.0 Parkfield earthquake, *Bull. Seismol. Soc. Am.*, *96*(4), S349–S363, doi:10.1785/0120050803.

Li, Y., G. P. De Pascale, M. C. Quigley, and D. M. Gravley (2014), Fault damage zones of the *M* 7.1 Darfield and *M* 6.3 Christchurch earthquakes characterized by fault zone trapped waves, *Tectonophysics*, *618*, 79–101, doi:10.1016/j.tecto.2014.01.029.

Li, Y. G., J. E. Vidale, and E. S. Cochran (2004), Low-velocity damaged structure of the San Andreas Fault at Parkfield from fault zone trapped waves, *Geophys. Res. Lett.*, *31*, L12S06, doi:10.1029/2003GL019044.

Lund Snee, J. E., V. G. Toy, and K. Gessner (2014), Significance of brittle deformation in the footwall of the Alpine Fault, New Zealand: Smithy Creek Fault zone, *J. Struct. Geol.*, *64*, 79–98, doi:10.1016/j.jsg.2013.06.002.

Malin, P. E., M. Lou, and J. A. Rial (1996), FR waves: A second fault-guided mode with implications for fault property studies, *Geophys. Res. Lett.*, *23*(24), 3547–3550, doi:10.1029/96GL03424.

Norris, R. J., and A. F. Cooper (1995), Origin of small-scale segmentation and transpressional thrusting along the Alpine Fault, New Zealand, *Geol. Soc. Am. Bull.*, *107*(2), 231–240.

Norris, R. J., and A. F. Cooper (2001), Late Quaternary slip rates and slip partitioning on the Alpine Fault, New Zealand, *J. Struct. Geol.*, *23*(2–3), 507–520, doi:10.1016/S0191-8141(00)00122-X.

Peng, Z., and Y. Ben-Zion (2006), Temporal changes of shallow seismic velocity around the Karadere-Duzce branch of the North Anatolian Fault and strong ground motion, *Pure Appl. Geophys.*, *163*(2–3), 567–600, doi:10.1007/s00024-005.0034-6.

Peng, Z., J. E. Vidale, M. Ishii, and A. Helmstetter (2007), Seismicity rate immediately before and after main shock rupture from high-frequency waveforms in Japan, *J. Geophys. Res.*, *112*, B03306, doi:10.1029/2006JB004386.

Petersen, T., K. Gledhill, M. Chadwick, N. H. Gale, and J. Ristau (2011), The New Zealand National Seismograph Network, *Seismol. Res. Lett.*, *82*(1), 9–20, doi:10.1785/gssrl.82.1.9.

Roland, E., and J. J. McGuire (2009), Earthquake swarms on transform faults, *Geophys. J. Int.*, *178*(3), 1677–1690, doi:10.1111/j.1365-246X.2009.04214.x.

Schuster, G. T., J. Yu, J. Sheng, and J. Rickett (2004), Interferometric/daylight seismic imaging, *Geophys. J. Int.*, *157*(2), 838–852, doi:10.1111/j.1365-246X.2004.02251.x.

Sibson, R. H., S. H. White, and B. K. Atkinson (1981), Structure and distribution of fault rocks in the Alpine fault zone, New Zealand, in *Thrust and Nappe Tectonics: International Conference*, edited by K. R. McClay and N. J. Price, pp. 197–210, Geol. Soc. London.

Sutherland, R. (1999), Basement geology and tectonic development of the greater New Zealand region: An interpretation from regional magnetic data, *Tectonophysics*, *308*(3), 341–362, doi:10.1016/S0040-1951(99)00108-0.

Sutherland, R., et al. (2012), Drilling reveals fluid control on architecture and rupture of the Alpine Fault, New Zealand, *Geology*, *40*(12), 1143–1146, doi:10.1130/G33614.1.

Townend, J., R. Sutherland, and V. Toy (2009), Deep Fault Drilling Project: Alpine Fault New Zealand, *Sci. Drill.*, *8*, 75–82, doi:10.2204/iodp.sd.8.12.2009.

Townend, J., R. Sutherland, V. G. Toy, J. D. Eccles, C. Boulton, S. C. Cox, and D. McNamara (2013), Late-interseismic state of a continental plate-bounding fault: Petrophysical results from DFDP-1 wireline logging and core analysis, Alpine Fault, New Zealand, *Geochem. Geophys. Geosyst.*, *14*, 3801–3820, doi:10.1002/ggge.20236.

Toy, V. G., et al. (2015), Fault rock lithologies and architecture of the central Alpine fault, New Zealand, revealed by DFDP-1 drilling, *Lithosphere*, doi:10.1130/L395.1.

van Avendonk, H. J. A., W. S. Holbrook, D. Okaya, J. K. Austin, F. Davey, and T. Stern (2004), Continental crust under compression: A seismic refraction study of South Island Geophysical Transect I, South Island, New Zealand, *J. Geophys. Res.*, *109*, B06302, doi:10.1029/2003JB002790.

Vidale, J. E., and Y. G. Li (2003), Damage to the shallow Landers fault from the nearby Hector Mine earthquake, *Nature*, *421*(6922), 524–526, doi:10.1038/nature01354.

Vidale, J. E., and P. M. Shearer (2006), A survey of 71 earthquake bursts across southern California: Exploring the role of pore fluid pressure fluctuations and aseismic slip as drivers, *J. Geophys. Res.*, *111*, B05312, doi:10.1029/2005JB004034.

Wech, A. G., C. M. Boese, T. A. Stern, and J. Townend (2012), Tectonic tremor and deep slow slip on the Alpine Fault, *Geophys. Res. Lett.*, *39*, L10303, doi:10.1029/2012GL051751.

Wells, A., M. D. Yetton, R. P. Duncan, and G. H. Stewart (1999), Prehistoric dates of the most recent Alpine fault earthquakes, New Zealand, *Geology*, *27*(11), 995–998.

Wu, J., and J. A. Hole (2011), Refraction of Fault-Zone Guided Seismic Waves, *Bull. Seismol. Soc. Am.*, *101*(4), 1674–1682, doi:10.1785/0120100024.

Wu, J., J. A. Hole, J. A. Snoke, and M. G. Imhof (2008), Depth extent of the fault-zone seismic waveguide: Effects of increasing velocity with depth, *Geophys. J. Int.*, *173*(2), 611–622, doi:10.1111/j.1365-246X.2008.03755.x.

Zoback, M., S. Hickman, and W. Ellsworth (2011), Scientific drilling into the San Andreas fault zone—An overview of SAFOD's first five years, *Sci. Drill.*, *1*, 14–28, doi:10.2204/iodp.sd.11.02.2011.